

Journal of Materials Chemistry A

Accepted Manuscript



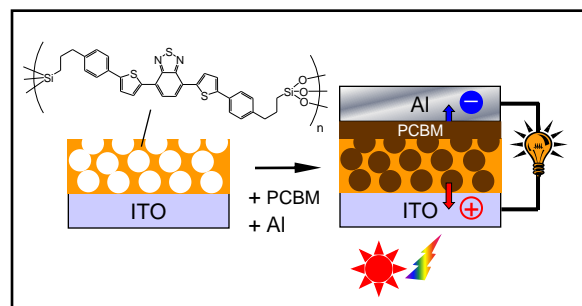
This is an *Accepted Manuscript*, which has been through the Royal Society of Chemistry peer review process and has been accepted for publication.

Accepted Manuscripts are published online shortly after acceptance, before technical editing, formatting and proof reading. Using this free service, authors can make their results available to the community, in citable form, before we publish the edited article. We will replace this *Accepted Manuscript* with the edited and formatted *Advance Article* as soon as it is available.

You can find more information about *Accepted Manuscripts* in the [Information for Authors](#).

Please note that technical editing may introduce minor changes to the text and/or graphics, which may alter content. The journal's standard [Terms & Conditions](#) and the [Ethical guidelines](#) still apply. In no event shall the Royal Society of Chemistry be held responsible for any errors or omissions in this *Accepted Manuscript* or any consequences arising from the use of any information it contains.

Table of contents entry



Mesoporous films containing 4,7-dithienyl-2,1,3-benzothiadiazole units in the frameworks were synthesized and demonstrated to function as a *p*-type layer for organic solar cells by filling an *n*-type PCBM in the mesopores.

Synthesis of visible-light-absorptive and hole-transporting periodic mesoporous organosilica thin films for organic solar cells

Cite this: DOI: 10.1039/x0xx00000x

Received 00th January 2012,

Accepted 00th January 2012

DOI: 10.1039/x0xx00000x

www.rsc.org/

Masamichi Ikai,^{‡,a,b,c} Yoshifumi Maegawa,^{‡,a,b,c} Yasutomo Goto,^{a,b,c} Takao Tani^{a,b} and Shinji Inagaki^{*,a,b,c}

Periodic mesoporous organosilica (PMO) thin films that possess both visible-light absorption and hole-transporting properties were synthesized from a newly designed 4,7-dithienyl-2,1,3-benzothiadiazole (DTBT)-bridged organosilane precursor using polystyrene-*block*-poly(ethylene oxide) (PS-*b*-PEO) as a template. DTBT-based PMO films were successfully obtained from the 100% organosilane precursor without the addition of other alkoxysilanes such as tetraethoxysilane and by control of the tetrahydrofuran/ethanol solvent ratio and the PS/PEO group ratio in the block copolymer. The PMO films possess connected cage-like mesopores with diameters of ca. 15–20 nm, which could be derived from templating with spherical micelles. The PMO films exhibited absorption in the visible range between 400 and 650 nm and hole-transport mobility in the order of $10^{-5} \text{ cm}^2 \text{ V}^{-1} \text{ s}^{-1}$. We demonstrate that the PMO thin film functions as a *p*-type layer for organic solar cells by filling an *n*-type [6,6]-phenyl C₆₁ butyric acid methyl ester into the mesopores.

Introduction

Periodic mesoporous organosilicas (PMOs), synthesized by surfactant-directed polycondensation of organic-bridged alkoxysilane precursors (R[Si(OR')₃]_{*n*}, where R = organic group and R' = Me, Et, *i*-Pr, etc., $n \geq 2$), are a new class of organic-inorganic hybrid materials with well-defined nanopores (2–30 nm) and high functionality attributed to the organic groups (R) fixed within the silicate frameworks.^{1,2} Desired framework functionalities can be constructed by molecular design of the organosilane precursors.² A number of PMOs with aromatic and π -conjugated bridging groups have been reported to have useful optical and electrical properties,^{2–6} such as strong fluorescence⁴, light harvesting capability⁵ and photocatalytic

electroactive π -conjugated tris(styryl)benzene.⁷ Hole-transporting PMOs have the potential to be utilized in optoelectronic devices due to their high surface area and well-controlled nanoporous structures. In particular, they have potential for application as the *p*-type layer in organic solar cells (OSCs)⁸ because well-defined interpenetrating *p-n* heterojunction structures can be constructed by filling the mesopores with an *n*-type material such as [6,6]-phenyl C₆₁ butyric acid methyl ester (PCBM).⁹

Very recently, Trauner and Bein first reported photovoltaic devices based on a porphyrin-based PMO and PCBM.¹⁰ Photovoltaic devices using photoactive covalent organic frameworks were also reported.¹¹ These reports revealed the potential application of organic-based nanoporous materials as the active layer of OSCs. However, the external quantum efficiency (EQE) of the porphyrin-PMO:PCBM device was limited to 0.035% or less with simulated solar irradiation. The nonlinear dependence of the steady-state current on the irradiation density revealed a transport-limit of the porphyrin-PMO devices, which resulted in non-geminate recombination at high light intensities and indicated very low hole mobility for the porphyrin-PMO film.

^a Toyota Central R&D Labs., Inc., Nagakute, Aichi 480-1192, Japan
E-mail: inagaki@mosk.tytlabs.co.jp

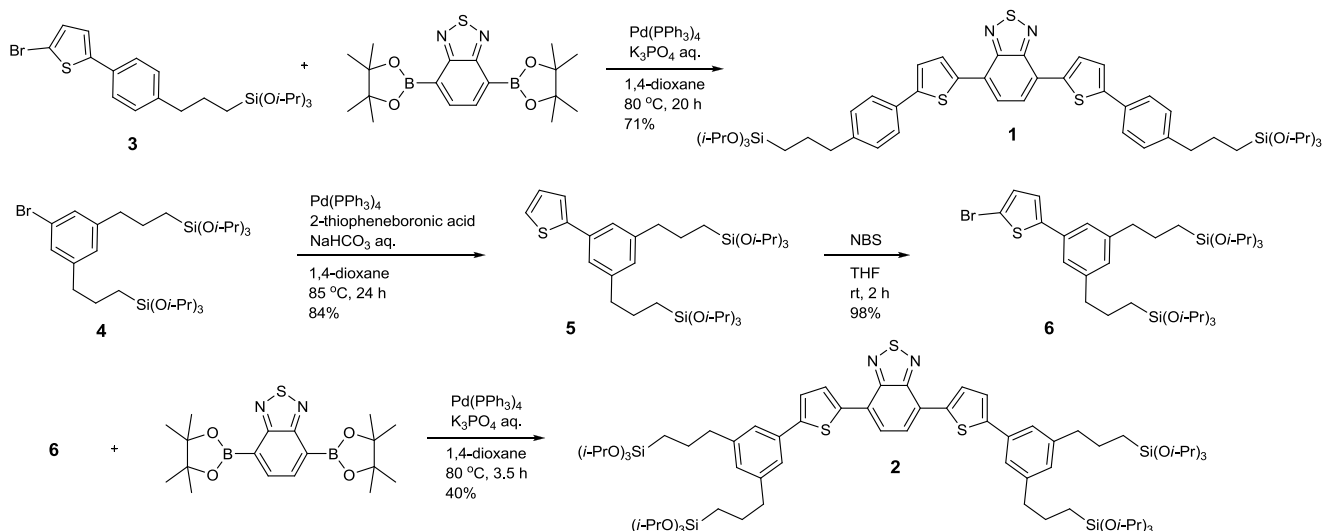
^b Core Research and Evolution Science and Technology (CREST), Japan Science and Technology Agency (JST), Japan

^c Advanced Catalytic Transformation program for Carbon utilization (ACT-C), Japan Science and Technology Agency (JST), Japan

† Electronic Supplementary Information (ESI) available: NMR spectra of organosilane precursors, krypton adsorption-desorption isotherm, pore size distribution of mesopores, UV-vis absorption spectra, ionization potential data and *J-V* characteristics of devices with/without a buffer layer. See DOI: 10.1039/b000000x/

‡ M. I. and Y. M. equally contributed to this article.
activity.⁶

We recently reported a hole-transporting PMO thin film synthesized from a three-armed organosilane precursor with an



Scheme 1 Synthesis route for two-armed and four-armed DTBT-bridged organosilane precursors **1** and **2**.

We have envisaged a strategy toward improvement of the PMO-based solar cell performance. Our approach is based on (i) the introduction of bridging organic groups which have high hole-transporting properties in the PMO framework, and (ii) the construction of large mesopores with diameters or ca. 15–20 nm to enable efficient infiltration of *n*-type materials into the mesopores. Toward this goal, we focused on 4,7-dithienyl-2,1,3-benzothiadiazole (DTBT) as a bridging organic group because the DTBT unit has attracted much attention recently for use in both polymer- and molecular-based OSCs due to its high hole mobility and wide range of visible-light absorption from the unique donor-acceptor-donor molecular structure.¹² In this study, two- and four-armed organosilane precursors were designed for preparation of the PMO films from the precursors without the addition of any pure silica precursors such as tetraethoxysilane (TEOS). For the synthesis of DTBT-PMO films with large mesopores, block copolymer (polystyrene-*block*-poly(ethylene oxide) (PS-*b*-PEO)) was used as a template in place of typical template surfactants such as alkyltrimethylammonium salts and tri- or di-block copolymers.

Here we report the successful synthesis of novel visible-light-absorptive and hole-transporting DTBT-bridged PMO films that possess connected cage-like mesopores with diameters of ca. 15–20 nm. The DTBT-PMO films exhibit a strong visible light absorption band with an edge at 650 nm and high hole-transportation. The OSC devices were fabricated by filling *n*-type PCBM into the large mesopores of the *p*-type DTBT-PMO films. DTBT-PMO:PCBM devices exhibited photovoltaic performance under visible light irradiation with a maximum EQE of 18%, which was more than 500 times higher than that for the previously reported porphyrin-PMO:PCBM device.

Results and Discussion

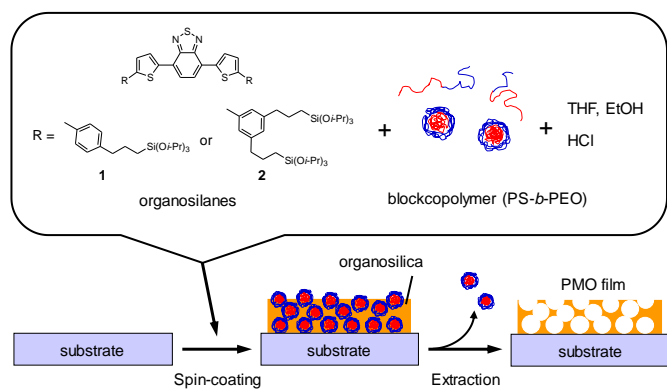
Synthesis of organosilane precursors

The DTBT-bridged alkoxy-silane precursors **1** and **2** with two or four alkoxy-silyl groups were synthesized as shown in Scheme

1. Synthesis of the precursors using a conventional synthetic approach was not easily accomplished, because the typical trimethoxy- and triethoxy-silyl groups were difficult to attach to the DTBT unit due to their high reactivity during the synthesis and purification steps. Therefore, the isopropoxysilyl group was employed as a silyl group rather than conventional silyl groups because it has sufficient stability for the cross-coupling reaction and purification using silica gel chromatography.¹³ Suzuki-Miyaura cross-coupling between molecular building blocks **3** or **6** and 2,1,3-benzothiadiazole-4,7-diboronic acid bis(pinacol) ester followed by purification with silica gel chromatography successfully afforded the precursors **1** or **2** in pure form (Figures S1 and S2, ESI†).

Preparation of PMO thin films

DTBT-PMO films were then synthesized by acidic sol-gel polymerization of the organosilane precursors in the presence of a block copolymer *via* evaporation-induced self-assembly (EISA) (Scheme 2). The reaction conditions and preparation procedure were carefully examined to obtain the desired PMO films because it was assumed that the bulky DTBT unit can weaken the interaction between the hydrolyzed silyl group and surfactant micelles to form a well-ordered mesostructure (Table 1). Sol mixtures containing precursor **1**, block copolymers **P1-P3**, and hydrochloric acid (HCl) in a reaction organic solvent were spin-coated on poly(3,4-ethylenedioxythiophene):poly(styrene sulfonic acid) (PEDOT:PSS)/indium tin oxide (ITO)/glass substrates (Scheme 2). After removal of the template, cross-sectional scanning electron microscopy (SEM) observations of the PMO films were conducted (Figure 1).



Scheme 2 Synthesis route for DTBT-based PMO films.

Table 1 Optimization of reaction conditions for the formation of well-defined PMO films.

Entry	Precursor	Block copolymer (M_n : PS- <i>b</i> -PEO / kg mol ⁻¹)	THF/EtOH (w/w)	PMO structure
1	1	P1 (20- <i>b</i> -14)	7/1	No formation
2		P1	3/1	Defined
3		P1	2/1	Disordered
4		P2 (20- <i>b</i> -6.5)	3/1	Disordered
5		P3 (58.6- <i>b</i> -71.0)	3/1	Well-defined
6	2	P3	2/1	Well-defined

Using **P1** ($M_n = 20\text{-}b\text{-}14 \text{ kg mol}^{-1}$) as a template, the solvent effect on the formation of well-ordered PMO structures was examined initially. The use of the tetrahydrofuran (THF)/ethanol (EtOH) (=7/1, w/w) mixed solvent had no effect on the formation of a well-ordered PMO film (Table 1, entry 1, Fig. 1a). However, the PMO structures did become easier to form with an increase in the ratio of EtOH to THF. For example, a well-defined structure was observed when the

solvent ratio of THF/EtOH was 3/1 (Table 1, entry 2, Fig. 1b). The pore sizes were estimated to be 15–20 nm, which is consistent with the shape of the spherical micelles of **P1**. This behavior can be explained by the stabilizing effect of the PS blocks in the presence of poor solvents such as EtOH and water.¹⁴ However, when the THF/EtOH solvent ratio was 2/1, vacant mesopores became unclear (Table 1, entry 3, Fig. 1c). Increasing the ratio of EtOH further (THF/EtOH=1/2) induced the precipitation of organosilica during preparation of the sol. This is considered to be caused by a weakening of the interactions between micelles and hydrolyzed precursors due to a decrease in silanol groups and/or unwanted consumption of precursors.

The influence of the size and ratio of PS and PEO groups in the block copolymers was investigated next. When the films were prepared from **P2** ($M_n = 20\text{-}b\text{-}6.5 \text{ kg mol}^{-1}$), it was very difficult to obtain spherical pore structures (Table 1, entry 4, Fig. 1d). This could be explained by the instability of the spherical micelles structures caused by the short hydrophilic PEO moiety.^{14a} In contrast, the use of **P3** ($M_n = 58.6\text{-}b\text{-}71.0 \text{ kg mol}^{-1}$) was effective for the formation of well-defined PMO films (denoted as **1-PMO-F**) (Table 1, entry 5, Fig. 1e). It is noteworthy that well-defined PMO films are obtained even if a two-armed organosilane precursor is used without the addition of any pure silica precursors. This is because stable micelles are formed during the EISA due to the long PEO moiety in **P3**. In the case of precursor **2**, well-defined PMO films (denoted as **2-PMO-F**) were easily obtained from the sol using the THF/EtOH mixed solvent with a ratio of 2/1 (Table 1, entry 6, Fig. 1f).

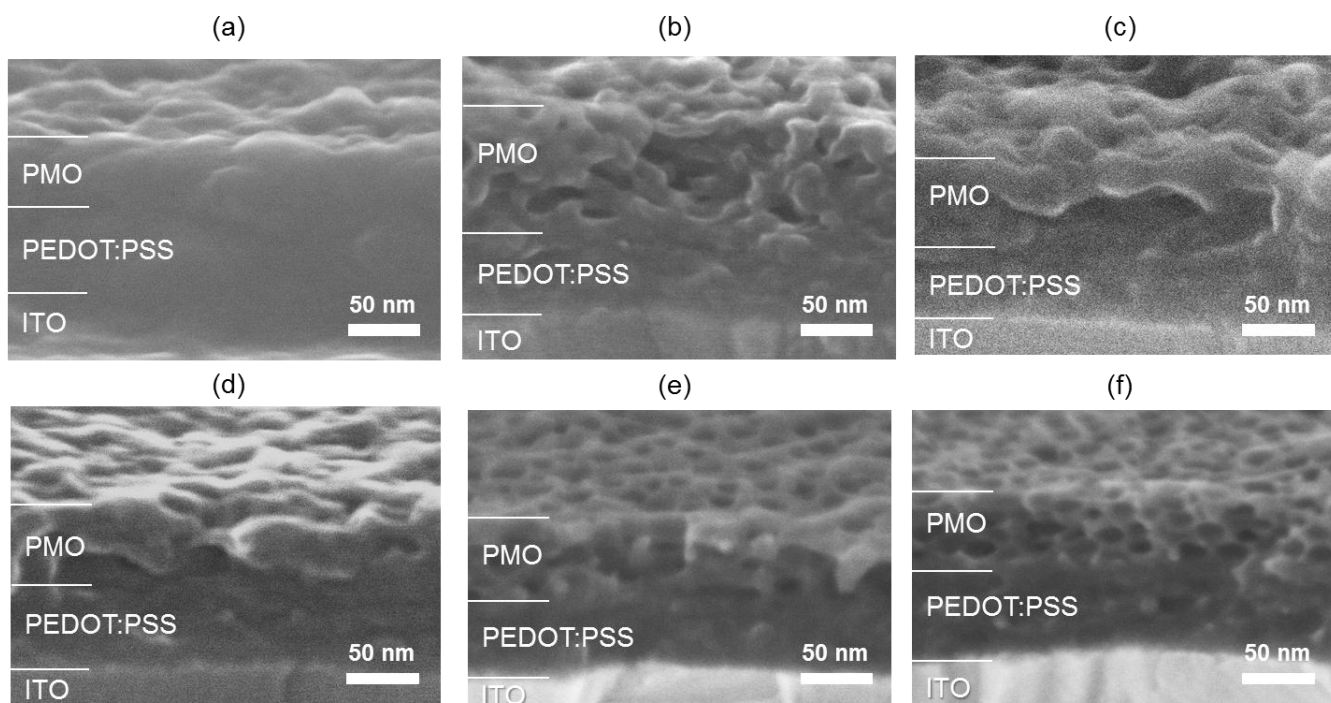


Fig. 1 Cross-sectional SEM images of PMO films. (a) to (f) correspond to entries 1 to 6 in Table 1.

Compared with **1-PMO-F**, the surface structure appears more isotropic, and well-ordered mesopores were formed. The ease of formation of the PMO structure can be attributed to the increased amount of silanol groups in the precursor.

Structural analysis of PMO thin films

Krypton adsorption, which is much more sensitive than nitrogen adsorption,¹⁵ was applied to assess surface area of **1-PMO-F** because the sample amount was too small to measure nitrogen adsorption due to very thin layer of PMO (~ 50 nm). The Brunauer–Emmett–Teller (BET) surface area of **1-PMO-F** calculated from the krypton adsorption isotherm was 285 m² g⁻¹ (Fig. S3, ESI†). The value is no large difference with that (225 m² g⁻¹) estimated from pore structures of SEM images (see ESI†). Unfortunately, the pore size distribution in the pore diameter range over ~ 9 nm cannot be determined from a krypton adsorption isotherm because pore condensation of krypton cannot be observed for pore diameters larger than 10 nm.¹⁵ Instead, the pore size distribution was obtained from top-view SEM images of **1-PMO-F** using an image analysis software (Figure S4, ESI†). The pores were distributed in narrow range with an average pore diameter of 15 nm and a standard deviation of 4 nm. The coefficient of variation (standard deviation / average pore diameter) is about 0.28. The value is similar to that (0.22) of a conventional PMO film which was estimated by the pore size distribution curve derived from nitrogen adsorption.¹⁶

2D-grazing incidence small-angle X-ray scattering (GI-SAXS) for **1-PMO-F** did not give helpful information on periodicity probably because the PMO layer is too thin to detect enough diffraction intensity.

UV-vis absorption properties

Figure 2 shows normalized UV-vis absorption spectra for DTBT-PMO films and their organosilane precursors (chloroform solution). Both of the PMO films and their precursor solutions exhibited absorption over a wide range from 300 to 650 nm. The absorption peaks at around 350 and 500 nm can be assigned to the π - π^* transition of the DTBT units and the intramolecular charge transfer between electron-rich thiophene and electron-deficient benzothiadiazole units, respectively.^{12b,17} These results support the successful incorporation of DTBT units into the PMO frameworks without loss of the absorption properties. The absorption bands for the PMO films at around 500 nm are broader than those for the precursor solutions,

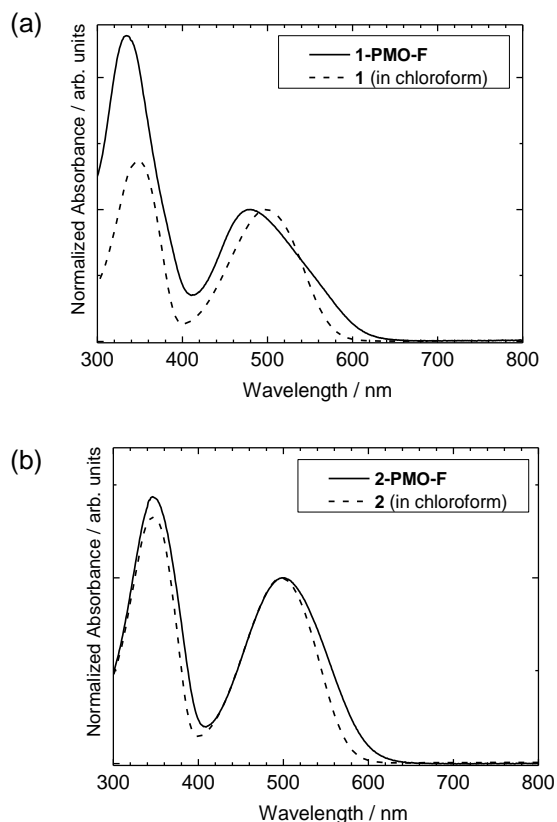


Fig. 2 Normalized UV-vis absorption spectra of (a) **1-PMO-F** (solid line) and precursor **1** (dashed line), (b) **2-PMO-F** (solid line) and precursor **2** (dashed line). The concentration of the chloroform solutions for precursors **1** and **2** was 10⁻⁵ M.

which suggests there are molecular interactions between DTBT units in the organosilica framework. In the case of **1-PMO-F**, the maximum wavelengths (λ_{\max}) of absorption spectra was blue-shifted with respect to that for corresponding precursor solutions, which could indicate the H aggregation of DTBT units within the organosilica framework. In contrast, λ_{\max} for **2-PMO-F** was primarily similar to that of the precursor solution, which suggests weak interaction between the DTBT groups in the ground state

Hole mobilities

Space-charge-limited current (SCLC) method was employed for measurement of the hole mobilities. Hole-only devices were fabricated by spin-coating of DTBT-silica films onto MoO₃-coated ITO/glass substrate and evaporation of a Au cathode onto the DTBT-silica films. Nonporous DTBT-silica films (**1-NP-F** and **2-NP-F**), which were prepared by spin-coating of a DTBT-sol mixture without template, were measured instead of the PMO films (**1-PMO-F** and **2-PMO-F**) because the Au

cathode could not be uniformly deposited onto the PMO films due to the highly porous structures. Very similar absorption spectra between the nonporous DTBT-silica films and the PMO films suggest similar optical and electrical properties for both films (Fig. 2 and Fig. S5, ESI†). Figure 3 shows the current density–voltage (J – V) characteristics of hole-only devices consisting of Au/1-NP-F/MoO₃/ITO/glass and Au/2-NP-F/MoO₃/ITO/glass. The hole mobilities for 1-NP-F and 2-NP-F were estimated to be 6×10^{-5} and 1.5×10^{-5} cm² V⁻¹ s⁻¹, respectively. The hole mobilities for the PMO films are comparable with that for a DTBT-based molecular film without silica (ca. 10^{-5} cm² V⁻¹ s⁻¹).^{12b} The higher mobility of 1-NP-F than 2-NP-F can be attributed to the lower content of insulating silica and alkylene moieties and/or stronger interaction between DTBT units (H aggregation), as suggested from the UV-vis spectra for 1-NP-F.

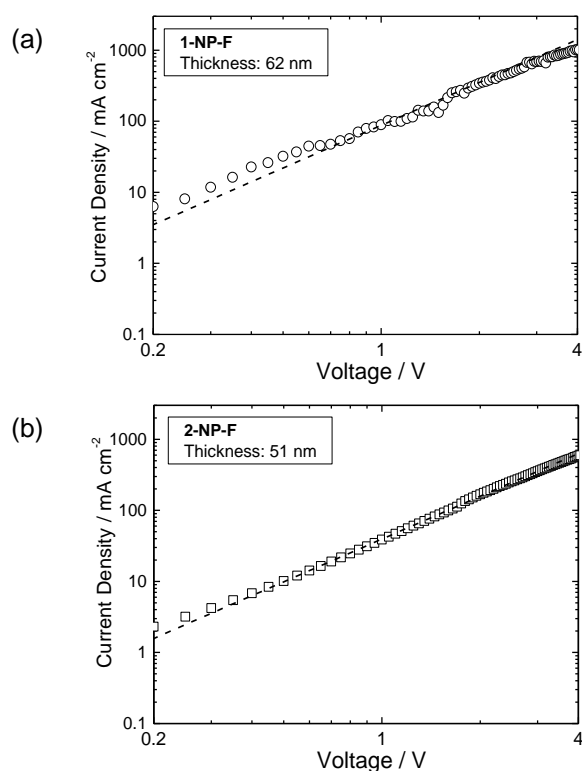


Fig. 3 J – V characteristics for hole-only devices with (a) 1-NP-F (film thickness: 62 nm, open circles) and (b) 2-NP-F (film thickness: 51 nm, open squares) films under the dark conditions. The dashed lines represent the prediction obtained using the SCLC model.

Photovoltaic performance of PMO-based OSCs

DTBT-PMO films were applied as a p -type active layer for the construction of OSCs. Figure 4a shows a schematic illustration of the fabrication steps for the DTBT-PMO-based OSCs. A buffer layer of nonporous two-armed DTBT-silica thin film (1'-NP-F) was inserted between the PMO film and PEDOT:PSS layers to prevent direct contact between PCBM filled in the mesopores and the PEDOT:PSS/ITO anode. After preparation of the PMO films (ca. 50 nm thickness) onto a buffer layer

coated PEDOT:PSS/ITO substrate, a chlorobenzene solution of PCBM was cast on top of the film and kept for a few minutes to infiltrate the PCBM solution into the mesopores. The excess solution was then removed by spinning the substrate. Figure 4b shows cross-sectional SEM images of the films before and after the infiltration of PCBM into the mesopores (top: 1-PMO-F, bottom: 2-PMO-F). The contrast attributable to vacant mesopores disappeared, which suggests that the mesopores are sufficiently filled with PCBM. LiF and Al were then deposited onto the PCBM layer as an electron extraction layer and cathode, respectively. The EQE and J – V characteristics of the devices were evaluated under 1 sun (AM 1.5G) simulated irradiation.

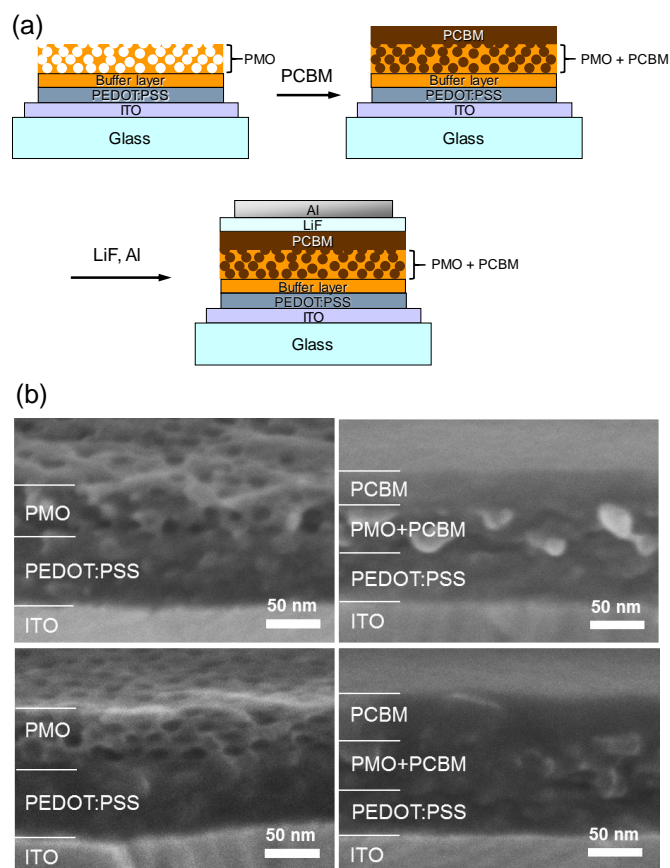


Fig. 4 (a) Schematic illustration of the fabrication steps for the OSC using p -type PMO film (orange) and PCBM (dark brown). (b) Cross-sectional SEM images of 1-PMO-F (top) and 2-PMO-F (bottom) on PEDOT:PSS/ITO before (left) and after (right) infiltration with PCBM.

Figure 5a shows the EQE spectra for devices based on 1-PMO-F:PCBM (device A) and 2-PMO-F:PCBM (device B). Both devices exhibited EQE spectra over a wide range of 300–650 nm with two peaks at around 340 and 480 nm. A comparison of the EQE spectrum with the UV-vis absorption spectra for DTBT-PMO and PCBM films (Fig. S6, ESI†) suggests that the carriers are generated from excitons both in PMO films and PCBM. The carriers generated from excitons at around 480 nm are mainly due to absorption by the DTBT-

PMOs. These results indicate that the PMO film can function as a *p*-type active layer for OSCs by filling the mesopores with an *n*-type material. The EQEs for **device A** reached 18% in the region of both wavelengths, while **device B** based on **2-PMO-F:PCBM** had EQE values of 5.5% at 340 nm and 4.3% at 480 nm. Notably, the EQEs of **device A** are more than 500 times higher than that of a conventional porphyrin-PMO:PCBM device.¹⁰ This large difference of EQE between these devices is possibly related to the high hole mobility of the DTBT-PMO films.

Figure 5b shows the *J*-*V* characteristics for the DTBT-PMO-based OSCs. The open circuit voltages (V_{OC}) for **device A** and **device B** were 0.91 V and 0.94 V, respectively.

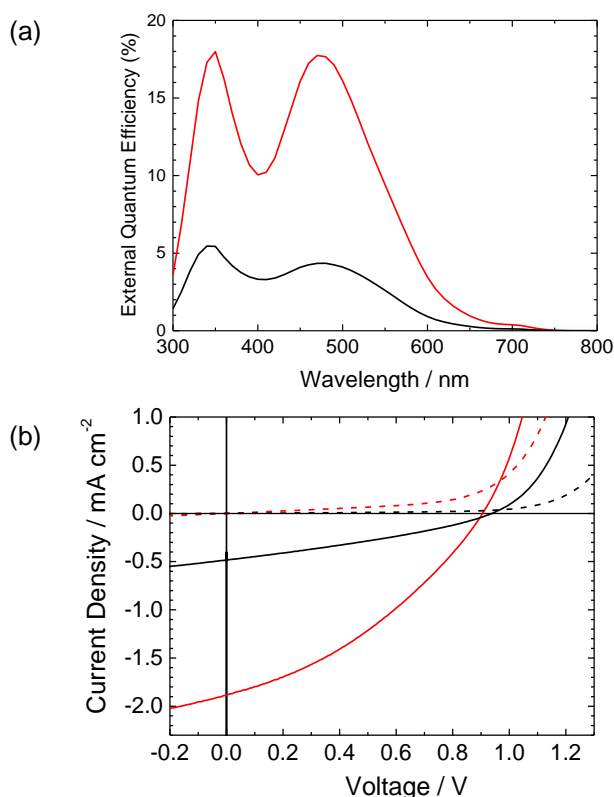


Fig. 5 (a) EQE and (b) *J*-*V* characteristics of the PMO-based OSCs (red: **device A**, black: **device B**) under 1 sun (AM 1.5G) simulated irradiation (solid lines) and in the dark (dashed lines).

The large V_{OC} values are attributable to the large ionization potential of the DTBT-PMO films (Fig. S7, ESI†). It should be noted that V_{OC} was significantly reduced when no buffer layer was inserted between the active layer and PEDOT:PSS (Fig. S8, ESI†). This is probably caused by leakage current due to the direct contacts between PEDOT:PSS/ITO anode and the PCBM filled in the mesopores.¹⁸ At negative voltages, the dark current for the device *without* a buffer layer was approximately an order of magnitude larger than that *with* a buffer layer (Fig. S4, ESI†), which indicates that the mesopores are filled with PCBM down to the interface between PEDOT:PSS and DTBT-PMO (**1-PMO-F** or **2-PMO-F**). The short circuit current

density (J_{SC}) and fill factor (FF) values for **device A** were 1.89 mA cm⁻² and 0.36, respectively. Thus, the power conversion efficiency (PCE) reached 0.61%. In contrast, the PCE for **device B** was only 0.14%, due to the low values of J_{SC} (0.48 mA cm⁻²) and FF (0.32). The lowered J_{SC} and FF can be explained mainly by the low hole mobility of **2-PMO-F** compared with **1-PMO-F**. It is considered that the molecular design of the organosilane precursor and the packing control of the electroactive organic units in the PMO framework should increase the hole mobility of the PMO active layer to achieve further improvement of the device performance. Thus, the design and synthesis of novel organosilane precursors and their PMO films are under further investigation by our group.

Conclusions

Visible-light-absorptive and hole-transporting PMO films with large pore size were successfully synthesized from newly designed organosilane precursors containing DTBT units and block copolymers as a template. The DTBT-PMO films were obtained from 100% DTBT-based organosilane precursors without the addition of another alkoxysilane such as TEOS by optimization of the reaction conditions. Well-defined and pore-size-controlled *p*-*n* heterojunction structures were constructed by filling the mesopores with an *n*-type material such as PCBM. DTBT-PMO-based OSCs were fabricated and showed a PCE of 0.61%, which demonstrates the DTBT-PMO films can function as a *p*-type active layer for OSCs.

Experimental

Materials

All reactions for organic synthesis were carried out under argon using standard high vacuum and Schlenk-line techniques. Unless otherwise noted, all chemicals, including dry solvents, were purchased from commercial suppliers (Sigma-Aldrich, Tokyo Chemical Industry Co., Ltd., and Wako Pure Chemical Industries Ltd.) and used without further purification. Compounds **3** and **4** were prepared according to the literature procedures.¹³ Block copolymers **P1** ($M_n = 20\text{-}b\text{-}14$ kg mol⁻¹, polydispersity index (PDI) = 1.08), **P2** ($M_n = 20\text{-}b\text{-}6.5$ kg mol⁻¹, PDI = 1.06), and **P3** ($M_n = 58.6\text{-}b\text{-}71.0$ kg mol⁻¹, PDI = 1.03) were purchased from Polymer Source, Inc. PCBM (nanom spectra E100H, purity > 99.5%) was purchased from Frontier Carbon. PEDOT:PSS (Clevios P) was purchased from H. C. Starck and passed through a 0.45 μm filter before spin-coating. High-purity (6N grade) MoO₃ was purchased from Mitsuwa Chemicals.

Methods

Nuclear magnetic resonance (NMR) spectra were recorded on a Jeol JNM-EXC400P spectrometer (400 MHz for ¹H and 100 MHz for ¹³C). Chemical shifts are reported in δ ppm referenced to an internal tetramethylsilane standard (δ 0.00) for ¹H NMR and chloroform-*d* (δ 77.0) for ¹³C NMR, respectively. Mass spectra were recorded on a Micromass GCT Premier mass

spectrometer (FI: field ionization and FD: field desorption). UV-vis absorption spectra were measured using a Jasco V-670 spectrometer. SEM images were obtained using a Hitachi S-5500 with an accelerating voltage of 2 or 10 kV. Krypton adsorption-desorption isotherms were measured using a Quantachrome Autosorb-1 at 87 K. Prior to measurements, all samples were outgassed at 80 °C for over 1 h in vacuum. Brunauer-Emmett-Teller (BET) surface areas were calculated from the linear section of the BET plot ($P/P_0 = 0.1-0.2$). For analyzing pore size distribution for mesopores in top-view SEM images of **1-PMO-F**, we used an image analysis software. Thicknesses of organosilica films for hole-only devices were measured by using a Dektak^{3ST} surface profilometer. Ionization potentials were measured by using a photo-electron spectrometer (AC-2, Riken Keiki). $J-V$ characteristics for the hole-only devices were measured by using a Keithley 2636A System SourceMeter. Both EQE and $J-V$ characteristics of solar cells were measured by using CEP-2000 (Bunkoukeiki). The $J-V$ characteristics were obtained under dark and white light illumination (simulated solar light, air mass (AM) 1.5G, 100 mW cm⁻²).

Synthetic procedures and Characterization

4,7-Bis(5-(4-(3-(triisopropoxysilyl)propyl)phenyl)thiophene-2-yl)-2,1,3-benzothiadiazole (1) : A 100 mL three-neck round-bottom flask connected to a condenser and dry argon flow was charged with a stir bar, compound **3** (378 mg, 0.77 mmol), 4,7-bis(4,4,5,5-tetramethyl-1,3,2-dioxaborolan-2-yl)-2,1,3-benzothiadiazole (143 mg, 0.37 mmol), potassium triphosphate (328 mg, 1.54 mmol), dry 1,4-dioxane (15 mL), and degassed distilled water (1.5 mL). After the mixture was stirred for 10 min at room temperature, Pd(PPh₃)₄ (44.5 mg, 38.5 μmol, 10 mol % Pd) was added one-portion under argon flow. The temperature was progressively raised to 80 °C and then the reaction mixture was stirred for 20 h. The reaction mixture was then concentrated under reduced pressure and the resulting crude residue was purified by flash chromatography (eluent: hexane/THF=40:1) affording **1** as a red tacky solid (246 mg, 71% yield). λ_{max} (chloroform)/nm 349 ($\epsilon/\text{dm}^3 \text{ mol}^{-1} \text{ cm}^{-1}$ 38800) and 499 (28400). ¹H NMR (400 MHz, CDCl₃) δ 0.64-0.68 (m, 4H), 1.20 (d, $J = 6.4$ Hz, 36H), 1.72-1.80 (m, 4H), 2.67 (br, 4H), 4.21 (sept, $J = 6.4$ Hz, 6H), 7.21 (d, $J = 8.4$ Hz, 4H), 7.35 (d, $J = 4.0$ Hz, 2H), 7.60 (s, $J = 8.4$ Hz, 4H), 7.80 (s, 2H), 8.05 (d, $J = 4.0$ Hz, 2H). ¹³C NMR (100 MHz, CDCl₃) δ 11.7, 25.0, 25.6, 39.0, 64.9, 123.5, 125.2, 125.7, 128.5, 129.1, 131.5, 138.1, 142.5, 145.74, 145.78, 152.5. FD-HRMS m/z calcd. for C₅₀H₆₈N₂O₆S₃Si₂ (M⁺): 944.3778; found: 944.3802.

1,3-Bis(3-(triisopropoxysilyl)propyl)-5-(thiophene-2-yl)benzene (5) : A 500 mL three-neck round-bottom flask connected to a condenser and dry argon flow was charged with a stir bar, compound **4** (4.85 g, 7.46 mmol), 2-thiopheneboronic acid (1.91 g, 14.9 mmol), sodium hydrogen carbonate (1.88 g, 22.4 mmol), dry 1,4-dioxane (100 mL), and degassed distilled water (10 mL). After the mixture was stirred for 10 min at room temperature, Pd(PPh₃)₄ (260 mg, 0.22 mmol, 3 mol % Pd) was

added one-portion under argon flow. The temperature was progressively raised to 85 °C and then the reaction mixture was stirred for 24 h. The reaction mixture was then concentrated under reduced pressure and the resulting crude residue was purified by silica gel chromatography (eluent: hexane/CH₂Cl₂=1:2) affording **5** as a transparent light yellow liquid (4.10 g, 84% yield). ¹H NMR (400 MHz, CDCl₃) δ 0.63-0.68 (m, 4H), 1.18 (d, $J = 6.4$ Hz, 36H), 1.71-1.79 (m, 4H), 2.64 (t, $J = 7.6$ Hz, 4H), 4.20 (sept, $J = 6.4$ Hz, 6H), 6.92 (s, 1H), 7.05 (dd, $J = 3.6$ Hz, 4.8 Hz, 1H), 7.23 (d, $J = 4.8$ Hz, 1H), 7.24 (s, 2H), 7.26 (d, $J = 3.6$ Hz, 1H). ¹³C NMR (100 MHz, CDCl₃) δ 11.8, 25.1, 25.6, 39.3, 64.8, 122.7, 123.6, 124.3, 127.8, 128.1, 134.0, 143.1, 145.0. FD-HRMS m/z calcd. for C₃₄H₆₀O₆SSi₂ (M⁺): 652.3649; found: 652.3662.

1,3-Bis(3-(triisopropoxysilyl)propyl)-5-(5-bromothiophene-2-yl)benzene (6) : A 100 mL two-neck round-bottom flask connected to dry argon flow was charged with a stir bar, the compound **5** (837 mg, 1.28 mmol), and dry THF (50 mL). After the mixture was stirred for 10 min at 0 °C, *N*-bromosuccinimide (320 mg, 1.80 mmol) was added one-portion under argon flow. The reaction mixture was stirred for 2 h at room temperature. The organic phase was washed with saturated NaHCO₃ aqueous solution and dried over anhydrous MgSO₄, filtered and concentrated under reduced pressure. The resulting crude residue was purified by silica gel chromatography (eluent: hexane/EtOAc=10:1) affording **6** as a transparent light yellow liquid (915 mg, 98% yield). ¹H NMR (400 MHz, CDCl₃) δ 0.62-0.66 (m, 4H), 1.18 (d, $J = 6.4$ Hz, 36H), 1.69-1.78 (m, 4H), 2.62 (t, $J = 7.6$ Hz, 4H), 4.19 (sept, $J = 6.4$ Hz, 6H), 6.93 (s, 1H), 7.00 (s, 2H), 7.13 (d, $J = 1.6$ Hz, 2H). ¹³C NMR (100 MHz, CDCl₃) δ 11.8, 25.1, 25.6, 39.2, 64.9, 110.8, 122.9, 123.3, 128.6, 130.6, 133.3, 143.3, 146.5. FD-HRMS m/z calcd. for C₃₄H₅₉BrO₆SSi₂ (M⁺): 730.2754; found: 730.2733.

4,7-Bis(5-(3,5-bis(3-(triisopropoxysilyl)propyl)phenyl)thiophene-2-yl)-2,1,3-benzothiadiazole (2) : A 100 mL three-neck round-bottom flask connected to a condenser and dry argon flow was charged with a stir bar, compound **6** (418 mg, 0.57 mmol), 4,7-bis(4,4,5,5-tetramethyl-1,3,2-dioxaborolan-2-yl)-2,1,3-benzothiadiazole (100 mg, 0.26 mmol), potassium triphosphate (120 mg, 0.57 mmol), dry 1,4-dioxane (20 mL), and degassed distilled water (2.0 mL). After the mixture was stirred for 10 min at room temperature, Pd(PPh₃)₄ (26.3 mg, 22.8 μmol, 4.0 mol % Pd) was added one-portion under argon flow. The temperature was progressively raised to 80 °C and then the reaction mixture was stirred for 30 min. Then, 4,7-bis(4,4,5,5-tetramethyl-1,3,2-dioxaborolan-2-yl)-2,1,3-benzothiadiazole (50 mg, 0.13 mmol) was added and the reaction mixture was stirred for 3 h. The reaction mixture was then concentrated under reduced pressure and the resulting crude residue was purified by flash chromatography (eluent: hexane/THF=40:1) affording **2** as a red tacky solid (166 mg, 40% yield). λ_{max} (chloroform)/nm 347 ($\epsilon/\text{dm}^3 \text{ mol}^{-1} \text{ cm}^{-1}$ 38600) and 497 (29100). ¹H NMR (400 MHz, CDCl₃) δ 0.66-0.70 (m, 8H), 1.20 (d, $J = 6.4$ Hz, 72H), 1.75-1.83 (m, 8H), 2.67 (t, $J = 7.6$ Hz, 4H), 4.21 (sept, $J = 6.4$ Hz, 12H), 6.96 (s, 2H), 7.35 (d, $J = 1.6$ Hz, 4H), 7.39 (d, $J = 4.0$ Hz, 2H), 7.89 (s, 2H), 8.11 (d,

$J = 4.0$ Hz, 2H). ^{13}C NMR (100 MHz, CDCl_3) δ 11.9, 25.1, 26.0, 39.3, 64.8, 123.6, 123.8, 125.2, 125.8, 128.5, 128.6, 133.8, 138.2, 143.2, 146.3, 152.6. FD-HRMS m/z calcd. for $\text{C}_{74}\text{H}_{120}\text{N}_2\text{O}_{12}\text{S}_3\text{Si}_4$ (M^+): 1436.7081; found: 1436.7035.

Preparation of sol mixtures and films

Unless otherwise specified, the sol mixtures described below were stirred (500 rpm) at 17–25 °C for 1 h. All of the sol mixtures described below were passed through 0.2 μm filter before casting on the substrates. Unless otherwise described, the sol mixtures were spin-coated onto each substrate at 4000 rpm for 30 s. Vapor treatments were conducted by storing the samples in a covered shallow plastic container where EtOH is placed.

Sol mixtures for entry 1-6 in Table 1: Precursor **1** or **2**, (5.0 mg) and the template block copolymer **P1** or **P2** (7.5 mg) or **P3** (5.0 mg) were dissolved in a mixture of THF and EtOH ((475.5 mg, entries 1-4, 7/1, 3/1, 2/1 or 3/1 (w/w), respectively) or (490 mg, entries 5-6, 3/1, or 2/1 (w/w), respectively)). After adding 4 M HCl aqueous solution (2.0 μL), the sol mixtures were stirred and then spin-coated onto each PEDOT:PSS/ITO substrate.

Sol A for 1-NP-F, Sol B for 2-NP-F: Precursor **1** or **2** (5.0 mg) was dissolved in a mixture of THF and EtOH (495 mg, sol A (3/1 (w/w)), sol B (2/1 (w/w))). After adding 4 M HCl aqueous solution (2.0 μL), the sol mixture was stirred.

Sol A' for a buffer layer (1'-NP-F): Precursor **1** (5.0 mg) was dissolved in THF (495 mg). After adding 12 M HCl aqueous solution (0.5 μL), the sol mixture was stirred. The obtained sol was diluted by adding THF and resulting in 0.125 wt% of sol mixture was prepared.

Sol C for 1-PMO-F, Sol D for 2-PMO-F: Precursor **1** or **2** (5.0 mg) and the template block copolymer **P3** (5.0 mg) were dissolved in a mixture of THF and EtOH (490 mg, sol C (3/1 (w/w)), sol D (2/1 (w/w))). After adding 4 M HCl aqueous solution (2.0 μL), the sol mixture was stirred.

1-NP-F or 2-NP-F on Si(100) for Ionization potential measurements: The film was formed on Si(100) substrate by spin-coating sol A or B at 3000 rpm for 30 s.

Fabrication methods of hole-only devices and the SCLC measurements

Hole-only devices were fabricated by using thermal evaporation onto cleaned glass substrates pre-coated with conductive, transparent ITO under high-vacuum conditions (the background pressure of the vacuum chamber was 5×10^{-7} Torr for MoO_3 and 1×10^{-7} Torr for electrode materials.). The glass substrates pre-coated with ITO (Sanyo Vacuum, thickness: 150 nm, sheet resistance: 10Ω square $^{-1}$) were cleaned ultrasonically in acetone and isopropyl alcohol. Prior to the MoO_3 deposition, the substrates were treated with UV-ozone, and immediately transferred into an evaporation chamber. A 10 nm-thick- MoO_3 was deposited on the substrates at a rate of 0.5 \AA s^{-1} . After the evaporation of MoO_3 , we spin-coated sol A or sol B onto the MoO_3 film to form DTBT-silica films (**1-NP-F** or **2-NP-F** (at 2000 rpm for 30 s)). After evaporating Au cathodes on the DTBT-silica films under high vacuum conditions, the hole-only

devices were encapsulated using a UV-epoxy resin and a glass plate under a nitrogen atmosphere.

We obtained the J - V characteristics for the hole-only devices. The hole mobilities are determined by fitting the J - V curves into Mott-Gurney's square law:

$$J = \frac{9}{8} \varepsilon_0 \varepsilon_r \mu \frac{V^2}{L^3}$$

where ε_0 is the permittivity of free space, ε_r is the relative permittivity of the materials (assuming $\varepsilon_r = 3.5$ for DTBT-silica films), μ is the hole mobility, V is the voltage drop across the device, and L is the thickness of the organosilica layer.

Fabrication methods of PMO-based solar cells

Device structures (device A or device B): Al (100 nm) / LiF (0.5 nm) / PCBM / (**1-PMO-F** or **2-PMO-F**) (ca. 50 nm) / **1'-NP-F** / PEDOT:PSS (50 nm) / ITO (150 nm) / glass

A PEDOT:PSS was spin-coated onto the ITO substrates after passing through 0.45 μm filter. The samples were annealed on a hot plate at 140 °C for 90 min. Then we formed a thin layer (**1'-NP-F**) as a buffer layer by casting 200 μL of sol A' on the PEDOT:PSS/ITO substrates and spinning the samples. The samples were stored in shallow plastic containers with a cover over night and dried in air to facilitate condensation of the buffer layers. Then we constructed a thin film as an active layer by casting 100 μL of sol C or D on the **1'-NP-F** layers and spinning the samples. After drying the samples in air by storing in the container with a cover over night, we formed PMO films by extracting the block copolymer **P3** twice in a heated toluene at 105 °C in an oven for 24 h. After the preparation of **1-PMO-F** or **2-PMO-F** on **1'-NP-F** / PEDOT:PSS/ITO substrates, the samples were heated at 50 °C for 5 min. Then, a 2 wt% chlorobenzene solution of PCBM (400 μL) at 50 °C was cast on top of the PMO films, and left for a few minutes to infiltrate the PCBM solution into the mesopores. The excess solution was then removed by spinning the substrate (at 1500 rpm, 30 s). Through a shadow mask, LiF (0.5 nm) and Al (150 nm) were then deposited onto the PCBM layer as an electron extraction layer and a cathode, respectively. The active area of the solar cells was 9 mm 2 . The solar cells were encapsulated using a UV-epoxy resin and a glass plate under a nitrogen atmosphere.

Acknowledgments

This work was partially supported by a Grant-in-Aid for Scientific Research on Innovative Areas "Artificial photosynthesis (AnAp-ple)" (No. 2406) from the Japan Society for the Promotion of Science (JSPS). The authors thank Shuji Kajiyama and Ken-ichi Yagi for FI-HRMS and FD-HRMS measurements and Kensuke Wada for his assistance on analyzing pore size distribution of mesopores.

Notes and references

- 1 (a) S. Inagaki, S. Guan, Y. Fukushima, T. Ohsuna and O. Terasaki, *J. Am. Chem. Soc.*, 1999, **121**, 9611.; (b) B. J. Melde, B. T. Holland, C. F. Blanford and A. Stein, *Chem. Mater.*, 1999, **11**, 3302.; (c) T. Asefa, M. J. MacLachlan, N. Coombs and G. A. Ozin, *Nature*, 1999, **402**, 867.
- 2 (a) F. Hoffmann, M. Cornelius, J. Morell and M. Fröba, *Angew. Chem. Int. Ed.*, 2006, **45**, 3216.; (b) W. Wang, J. E. Lofgreen and G. A. Ozin, *Small*, 2010, **6**, 2634.; (c) N. Mizoshita, T. Tani and S. Inagaki, *Chem. Soc. Rev.*, 2011, **40**, 789.
- 3 (a) C. Yoshina-Ishii, T. Asefa, N. Coombs, M. J. MacLachlan and G. A. Ozin, *Chem. Commun.*, 1999, 2539.; (b) S. Inagaki, S. Guan, T. Ohsuna and O. Terasaki, *Nature*, 2002, **416**, 304.; (b) P. N. Minoofar, B. S. Dunn and J. I. Zink, *J. Am. Chem. Soc.*, 2005, **127**, 2656.; (c) E. Johansson and J. I. Zink, *J. Am. Chem. Soc.*, 2007, **129**, 14437.; (d) W. Whitnall, L. Cademartiri and G. A. Ozin, *J. Am. Chem. Soc.*, 2007, **129**, 15644.; (e) M. A. Wahab, S. Sudhakar, E. Yeo and A. Sellinger, *Chem. Mater.*, 2008, **20**, 1855.; (f) M. Cornelius, F. Hoffmann, B. Ufer, P. Behrens and M. Fröba, *J. Mater. Chem.*, 2008, **18**, 2587.; (g) N. Mizoshita, T. Tani, H. Shinokubo and S. Inagaki, *Angew. Chem. Int. Ed.*, 2012, **51**, 1156.
- 4 (a) Y. Goto, N. Mizoshita, O. Ohtani, T. Okada, T. Shimada, T. Tani and S. Inagaki, *Chem. Mater.*, 2008, **20**, 4495.; (b) N. Mizoshita, Y. Goto, T. Tani and S. Inagaki, *Adv. Funct. Mater.* 2008, **18**, 3699.; (c) N. Mizoshita, Y. Goto, M. P. Kapoor, T. Shimada, T. Tani and S. Inagaki, *Chem. Eur. J.* 2009, **15**, 219.; (d) T. Tani, N. Mizoshita and S. Inagaki, *J. Mater. Chem.*, 2009, **19**, 4451., and references therein.; (e) N. Mizoshita, Y. Goto, Y. Maegawa, T. Tani and S. Inagaki, *Chem. Mater.*, 2010, **22**, 2548.
- 5 (a) S. Inagaki, O. Ohtani, Y. Goto, K. Okamoto, M. Ikai, K. Yamanaka, T. Tani and T. Okada, *Angew. Chem. Int. Ed.*, 2009, **48**, 4042.; (b) H. Takeda, Y. Goto, Y. Maegawa, T. Ohsuna, T. Tani, K. Matsumoto, T. Shimada, S. Inagaki, *Chem. Commun.* 2009, 6032.; (c) Y. Maegawa, N. Mizoshita, T. Tani and S. Inagaki, *J. Mater. Chem.*, 2010, **20**, 4399.
- 6 (a) M. Ohashi, M. Aoki, K. Yamanaka, K. Nakajima, T. Ohsuna, T. Tani and S. Inagaki, *Chem.-Eur. J.*, 2009, **15**, 13041.; (b) H. Takeda, M. Ohashi, T. Tani, O. Ishitani and S. Inagaki, *Inorg. Chem.*, 2010, **49**, 4554.
- 7 N. Mizoshita, M. Ikai, T. Tani and S. Inagaki, *J. Am. Chem. Soc.*, 2009, **131**, 14225.
- 8 (a) G. Yu, J. Gao, J. C. Hummelen, F. Wudl and A. J. Heeger, *Science*, 1995, **270**, 1789.; (b) J. Peet, A. J. Heeger and G. C. Bazan, *Acc. Chem. Res.*, 2009, **42**, 1700., and references therein.; (c) C. J. Brabec, V. Dyakonov and U. Scherf, In *Organic Photovoltaics: Materials, Device Physics, and Manufacturing Technologies*., John Wiley & Sons: 2008.
- 9 M. Ikai, Y. Maegawa, N. Mizoshita, T. Tani and S. Inagaki, Solar cell and method for manufacturing the same., *Japanese Patent*, JP 5110399, 2012.
- 10 Y. Li, F. Auras, F. Löbermann, M. Döblinger, J. Schuster, L. Peter, D. Trauner and T. Bein, *J. Am. Chem. Soc.*, 2013, **135**, 18513.
- 11 (a) M. Dogru, M. Handloser, F. Auras, T. Kunz, D. Medina, A. Hartschuh, P. KnocheI, T. Bein, *Angew. Chem. Int. Ed.*, 2013, **52**, 2920.; (b) J. Guo, Y. Xu, S. Jin, L. Chen, T. Kaji, Y. Honsho, M. A. Addicoat, J. Kim, A. Saeki, H. Ihee, S. Seki, S. Irlle, M. Hiramoto, J. Gao and D. Jiang, *Nat. Commun.* 2013, **4**, 2736.
- 12 (a) J. W. Chen and Y. Cao, *Acc. Chem. Res.*, 2009, **42**, 1709., and references therein.; (b) Z. Wu, B. Fan, F. Xue, C. Adachi and J. Ouyang, *Sol. Energy Mater. and Sol. Cells*, 2010, **94**, 2230.
- 13 Y. Maegawa, M. Waki, A. Umamoto, T. Shimada and S. Inagaki, *Tetrahedron*, 2013, **69**, 5312.
- 14 (a) K. Yu and A. Eisenberg, *Macromolecules*, 1996, **29**, 6359.; (b) Y. -J. Cheng and J. S. Gutmann, *J. Am. Chem. Soc.*, 2006, **128**, 4658.; (c) D. Chandra, T. Ohji, K. Kato and T. Kimura, *Phys. Chem. Chem. Phys.*, 2011, **13**, 12529.; (d) A. F. M. Barton, *CRC Handbook of Polymer-Liquid Interaction Parameters and Solubility Parameters*. CRC Press, Boca Raton: 1990.
- 15 M. Thommes, N. Nishiyama and S. Tanaka, *Studies in Surf. Sci. and Catal.*, 2007, **165**, 551.
- 16 N. Mizoshita, K. Yamanaka, T. Shimada, T. Tani and S. Inagaki, *Chem. Comm.*, 2010, **46**, 9235. The value of 0.22 was estimated from inset data of Fig. S7 in ESI.
- 17 (a) K. G. Jespersen, W. J. D. Beenken, Y. Zaushitsyn, A. Yartsev, M. Andersson, T. Pullerits and V. Sundström, *J. Chem. Phys.*, 2004, **121**, 12613.; (b) S. Roquet, A. Cravino, P. Leriche, O. Alévêque, P. Frère and J. Roncali, *J. Am. Chem. Soc.*, 2006, **128**, 3459.
- 18 (a) A. W. Hains and T. J. Marks, *Appl. Phys. Lett.*, 2008, **92**, 023504.; (b) N. Li, B. E. Lassiter, R. R. Lunt, G. Wei and S. R. Forrest, *Appl. Phys. Lett.*, 2009, **94**, 023307.; (c) M. D. Perez, C. Borek, S. R. Forrest and M. E. Thompson, *J. Am. Chem. Soc.*, 2009, **131**, 9281.